Role of boundary roughness in the electronic transport of Bi nanowires

Authors: T.E. Huber, A. Nikolaeva, D. Gitsu, L. Konopko, Michael J. Graf

Published in *Journal of Applied Physics*, vol. 104, no. 12, 2008

Role of boundary roughness in the electronic transport of Bi nanowires

T. E. Huber, A. Nikolaeva, D. Gitsu, L. Konopko, and M. J. Graf

Citation: Journal of Applied Physics **104**, 123704 (2008); doi: 10.1063/1.3041491
View online: http://dx.doi.org/10.1063/1.3041491
View Table of Contents: http://scitation.aip.org/content/aip/journal/jap/104/12?ver=pdfcov
Published by the AIP Publishing

Role of boundary roughness in the electronic transport of Bi nanowires

T. E. Huber,[1,a)] A. Nikolaeva,[2,3] D. Gitsu,[2] L. Konopko,[2,3] and M. J. Graf[4]
[1]*Howard University, Washington, DC 20059, USA*
[2]*Institute of Electronic Engineering and Industrial Technologies, ASM, Chisinau MD-2028, Moldova*
[3]*International High Magnetic Field and Low Temperatures Laboratory, Wroclaw 53-421, Poland*
[4]*Department of Physics, Boston College, Chestnut Hill, Massachusetts 02467, USA*

(Received 17 June 2008; accepted 29 October 2008; published online 17 December 2008)

We present a study of electronic transport in 200 nm diameter bismuth nanowire arrays embedded in an alumina matrix where the nanowires are oriented preferentially with the trigonal crystalline axis parallel to the wire length. The study is based on measurements of the resistance and thermopower over a wide range of temperatures (4–300 K) as well as of magnetoresistance for fields of up to 9 T. The Fermi energies are obtained from the Landau level spectrum; results show that the wires have the intrinsic electron and hole concentrations. At high temperatures, the mobilities are temperature dependent and the electron mobility is several orders of magnitude larger than that of holes. This nanowire mobility behavior, which is also observed in the bulk, is attributed to carrier-phonon scattering. At low temperatures, the mobilities are temperature independent and roughly the same for electrons and holes. An interpretation in terms of boundary roughness scattering is proposed. © *2008 American Institute of Physics*. [DOI: 10.1063/1.3041491]

I. INTRODUCTION

Thin films and one-dimensional materials, such as nanowires (NWs) and nanotubes,[1,2] have attracted considerable attention in theoretical and experimental studies. Hicks and Dresselhaus[3] showed that electronic property modifications induced by quantum confinement in NWs can be used to overcome the solid-state heat-electric (thermoelectric) efficiency barriers imposed by the physics of bulk materials. Bismuth (Bi) is a well known thermoelectric material in its bulk form,[4] which, having a long Fermi wavelength ($\lambda_F \sim 50$ nm), exhibits strong quantum confinement effects in NWs, i.e., a semimetal-to-semiconductor transition. Therefore, the investigation of low dimensional Bi has become a very active field.[5–14] The Fermi surface and electronic band structure of bulk bismuth are shown in Fig. 1.

Even though the interesting quantum confinement effects in Bi NWs occur for diameters $d \sim \lambda_F$, the first physical limit that is reached is related to the mean free path (mfp) of the charge carriers. When the NW diameter or film thickness is less than the mfp, charge carrier scattering at the nanostructure boundary becomes comparable to intrinsic scattering, and the scattering time and mobility of the charge carriers are, in general, reduced. Thus, the electrical resistivity of the material in the nanostructure will increase from the bulk value. This is the finite-size effect of the resistance. Nikolaeva, Huber, Gitsu, and Konopko (NHGK) recently presented a study of electronic transport in individual Bi NWs whose diameter was large relative to the Fermi wavelength.[15] NHGK's study[15] was based on measurements of the resistance and thermopower of intrinsic and Sn-doped Bi single-crystal individual NWs grown using the Ulitovski method for various wire diameters in the range 150–480 nm. These measurements were carried out over a wide range of temperatures (4–300 K) and magnetic fields (0–14 T). It was found that the thermopower of intrinsic Bi wires in this diameter range is positive (type *p*) below about 150 K, displaying a peak at around 40 K. This is in sharp contrast with the typical situation in bulk bismuth. With the exception of temperatures below 10 K,[16–18] the thermopower of bulk Bi is due to the difference in broadening of the Fermi distribution between hot and cold regions of the sample or diffusion thermopower with the electron mobility, μ, much larger than the hole mobility, ν; that is, the diffusive thermopower of bulk Bi is negative or type *n*.[19–23] The scattering mechanism in bulk Bi is charge-phonon scattering.[24] NHGK's measurements[15] were interpreted in terms of the model of the diffusive thermopower model, and as a result we obtained the diameter-dependent, temperature-dependent mobilities of electrons and holes. As far as finite-size effects, NHGK (Ref. 15) found that the carrier mobilities are limited by a temperature-independent term that is roughly the same for the two carriers. Although individual Bi NWs are ideal systems for transport and thermopower studies, most of the bismuth electronic transport studies have been carried out in nanowire arrays (NWAs), and therefore, we are motivated to investigate finite-size effects on the thermopower of NWAs.

Another motivation to study NWA is as follows. Bi NWs are anisotropic. The anisotropy of the bulk physical properties of crystals has been discussed by Nye.[25] In the case of bulk Bi there are two electron mobilities μ_1 and μ_3 and two hole mobilities ν_1 and ν_3. Because of the crystalline orientation of the Ulitovski individual Bi NWs, their transport properties are dominated by μ_1 and ν_1, the mobilities in the basal plane. In contrast, the thermopower of the NWs in the NWAs that we present in this work, whose crystalline orientation with respect to the wire length is roughly perpendicular to that of the individual Bi NWs, is dominated by μ_3 and ν_3

a)Electronic mail: thuber@howard.edu.

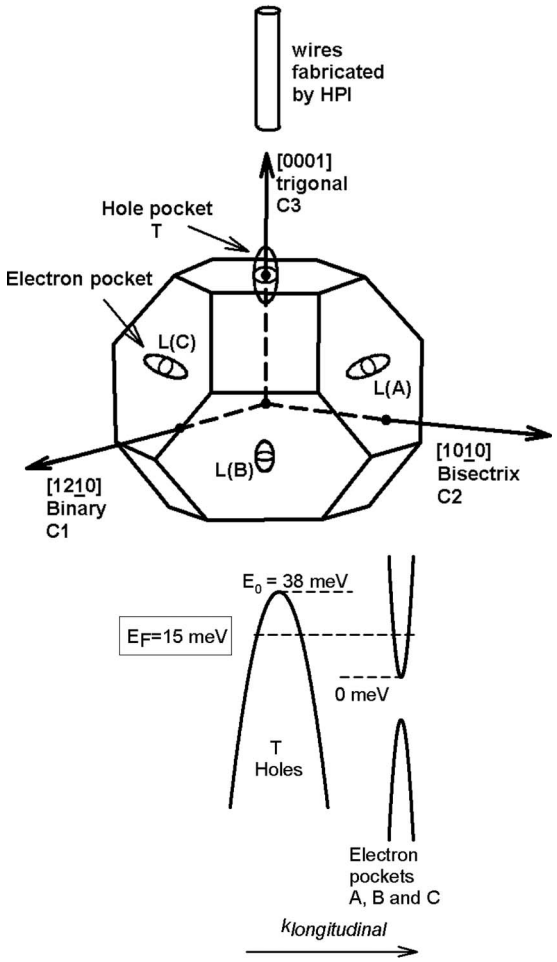

FIG. 1. (Top) The Brillouin zone for Bi, showing symmetry lines, which are indexed in the hexagonal system, and planes. The three Fermi surface electron pockets (*LA*, *LB*, and *LC*) and the *T*-hole pocket are also represented. The orientation of the trigonal wires is also indicated. (Bottom) Schematic energy band diagram of bismuth showing the Fermi level and the energies of the band edges of the electron and hole pockets. The energies are represented as a function of the longitudinal wavevector.

that are the mobilities across the basal plane. Therefore, the present study allows us to cover a fundamentally different set of mobilities than those studied by NHGK.[15]

Heremans and Thrush[6] studied the thermopower of 200 nm Bi NWAs. In that investigation the undoped samples show a type *p* behavior at low temperatures, which the authors interpreted in terms of phonon drag, in sharp contrast to the interpretation of the thermopower of individual NWs by NHGK.[15] The present article also seeks to clarify this issue.

It is expected that for NWs where $d > \lambda_F$, as in the present study, quantum confinement size effects are small. For very small diameter wires confinement causes the energies associated with transverse motion to be quantized, and the lowest energy level is increased, which results in an increase in the overlap energy between electron and hole bands E_0, 38 meV. For 200 nm wires, one expects $\Delta E_0 \sim 1-2$ meV with $\Delta E_0 \ll E_0$.[10] Our magnetoresistance measurements include the observation of Shubnikov–de Haas (SdH) oscillations, the analysis of which presents the additional benefit of allowing us to rule out unintentional doping that can occur during the manufacture of the NWs.

A theoretical study of the finite-size effect in wires, based on the work by Fuchs[26] and Sondheimer[27] on thin films, was presented by Dingle.[28] He found that the effect depends on *d*, mfp, and the specularity ε of scattering processes at the wire surface. This theory provides a basis for interpretation of NW size effects in a wide range of cases from bismuth NWs to copper NWs.[29] However, this time-honored approach to finite-size effects does not consider the mechanisms for boundary-carrier scattering. In this approach, mfp and ε are adjustable parameters. More recent theoretical studies of boundary-induced scattering in thin films by Calecki and co-workers[30–32] indicate that the boundary surface roughness at the nanoscale and the quantum-mechanical properties of the charge carriers are important. Roughness is sensed differently by quasiparticles according to their de Broglie wavelength and therefore the size effect is a quantum-mechanical phenomenon. The theoretical work makes specific predictions about the dependence of the mobility on carrier mass according to the roughness of the surface. Specifically, under very general conditions, the mobilities are independent of carrier mass. The trigonal Bi NWs in the present investigation are very promising for exploring this property because, for this orientation, the ratio of the hole longitudinal mass to electron longitudinal mass is 35. The issue of mass dependences has not been studied in other NWs or films and our results may suggest strategies for minimizing finite-size effects in nanostructures.

The paper is been organized as follows: In Sec. II, we briefly describe the sample fabrication and characterization processes. In Sec. III we present the procedure for the electronic transport and thermopower measurements as well as the experimental results of electronic transport including those results obtained using the SdH method. In Sec. IV we present the result of our thermopower measurements as well as a model of diffusion thermopower, which is based on a model of mobilities in NWs. Section V presents a discussion of the experimental results in terms of boundary scattering theories. Section VI concludes and summarizes the paper.

II. SAMPLE PREPARATION AND STRUCTURAL CHARACTERIZATION

Bi NW arrays are fabricated by the template injection technique as described in detail elsewhere.[7] The alumina templates used in this work are sold commercially for microfiltration under the trade name Anopore (Whatman, Clifton, NJ) and are made by the anodization of aluminum; they have a 200 nm channel diameter. The template consists of an alumina plate that is about 55 μm thick, which supports an array of parallel, largely noninterconnected, cylindrical channels running perpendicular to the plate surface. Careful examination shows that the mesoscopic morphology of the template is complex. The channel structure is slightly asymmetric, with the channels tapering toward the plate surface that was originally in contact with the aluminum metal. The channel ends are also irregular on this side, over a distance of about 2 μm from the surface. The channels are funnel shaped with channel diameters, on opposite sides of the anodic plate of 235 ± 30 nm and 310 ± 40 nm, after removal of the 2 μm thick surface layer. Figure 2(a) shows a scan-

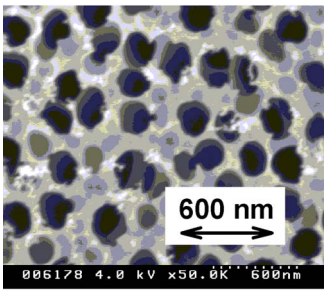

(a)

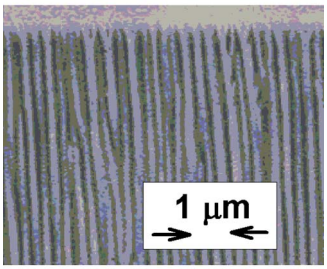

(b)

FIG. 2. (Color online) (a) SEM top view of the 200 nm porous anodic aluminum Anopore template. The electron energy is 4 keV. The alumina appears as light areas; the dark areas are nanochannels. (b) SEM cross section of a 200 nm (nominal) wire array. The wires appear as the light areas; the dark areas are the insulating matrix. The very light area at the top, which spans the width of the image, is the top of the array and consists of bulk Bi; this layer constitutes the cap. The electron energy is 2 keV and the magnification is 5000.

ning electron microscope (SEM) image of the template and Fig. 2(b) shows a SEM image of a cross section of the NW array sample. An x-ray diffraction (XRD) spectrum of a Bi-NWA is shown in Fig. 3. The XRD spectra peaks were very

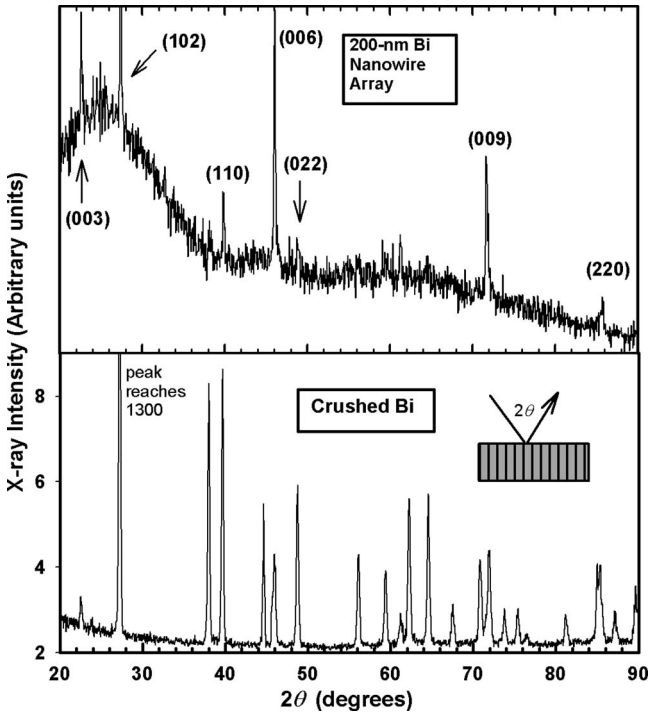

FIG. 3. XRD spectra of a Bi NWA with a diameter of 200 nm (top) and of bulk Bi powder (bottom). The inset shows the geometry employed for the scans.

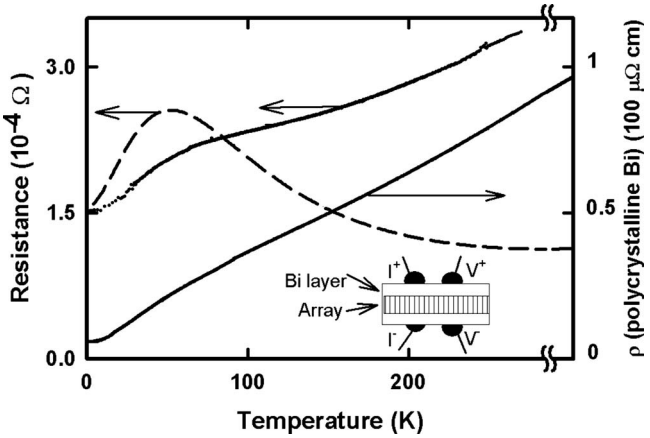

FIG. 4. Resistance of the 200 nm (nominal) wire array and the resistivity of a sample polycrystalline Bi material. The inset shows a schematic of the arrangement of electrodes used for the transport measurements. The resistance that results from our model is shown with dashed lines; this resistance has arbitrary units as it is set to match the resistance of the NW at low temperatures.

narrow, which indicated a long-range periodicity of the structure along the wire length. The positions of the observed peaks corresponded within the experimental resolution (0.2°) to those for the bulk, indicating that the rhombohedral crystal structure of bulk Bi is preserved in the NWs. The appearance of only a few peaks of the rhombohedral structure suggested that individual wires are composed of highly oriented crystalline grains. The prominence of the (003), (006), and (009) peaks relative to the (102) peak indicated that the crystal grains are oriented with the trigonal axis along the wire length, since the scattering geometry employed probes only at interplanar distances along the wire's length. We estimate that any changes in the lattice parameters $(\Delta a/a)$ would be $<1.7\times10^{-3}$. By comparison, the Bi NWAs by NHGK (Ref. 15) were oriented along a crystal direction perpendicular to the (202) lattice plane, i.e., the wire axis lies along a trigonal-bisectrix plane and close to the bisectrix.

III. ELECTRONIC TRANSPORT RESULTS

Measurements of the zero-field resistance and of the magnetoresistance of the samples were made in a cryostat operating in a temperature range of 1.8–300 K. Transport measurements on the samples are essentially two-point measurements, and the measured resistance contains a contribution from the resistance at the boundary between the contact material and the Bi NW caused by the contact resistance of the individual NWs that depends on the contact area and also, effectively, on the number of wires that are contacted. In the electronic transport studies we used two different approaches for minimizing the impact of contacts on the measurements (thermopower will be discussed separately). In one approach, the NWs are capped with a layer of Bi; a SEM image of the boundary between the NWs and the bulk is shown in Fig. 4. The contact resistance is small. A study of the temperature-dependent resistance and magnetoresistance of the capped samples shows that we achieve a residual (low-temperature) contact resistance of 10^{-4} Ω or less. This is consistent with the single-NW results, taking into account

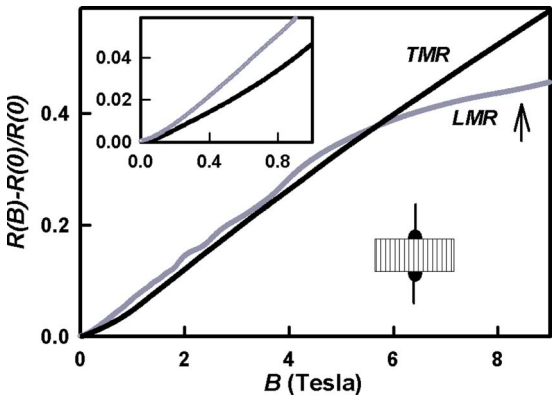

FIG. 5. (Color online) LMR and TMR of the 200 nm (nominal) Bi wire array as a function of magnetic field at low temperatures (2 K). The vertical arrow indicates the 1^- hole feature.

that the array consists of $\sim 10^8$ wires in parallel where the resistance of the wires is estimated to be 2 kΩ based on the bulk resistivity of Bi and the geometric parameters of the individual NWs. The other approach is to make contact using silver epoxy; these samples are termed "uncapped." This sample configuration is shown in the inset of Fig. 4. The measured resistance of the sample was around 100 Ω, which indicates that only a small number of NWs (~20) are contacted. The low probability of contact with silver epoxy is very well known.[33] Because of this feature, capped samples are much preferred over uncapped samples for determination of Bi NW resistance. Figure 4 shows the temperature-dependent resistance, $R(T)$, of the 200 nm sample with caps.

The magnetoresistance $\mathrm{MR}=[R(B)-R(0)]/R(0)$ for the capped sample exhibits artifices related to current jetting in the presence of a magnetic field. The appendix of Ref. 10 discusses this phenomenon. Therefore, we employ the uncapped configuration to study the magnetoresistance. The longitudinal magnetoresistance (LMR) is measured with the magnetic field parallel to the wire length, while for the transverse magnetoresistance (TMR) the field is perpendicular to the wire length. Figure 6 shows the LMR and TMR at 1.8 K for fields up to 9 T. Both the LMR and TMR increase with magnetic fields. For higher magnetic fields, the LMR saturates and becomes smaller than the TMR. In comparison, capped samples show a broad maximum in approximately the same magnetic field. These features can be interpreted in terms of Chambers' effect.[34,35] At field values below a crossover field B_C, carrier scattering at the wire boundary dominates, and the resistance is high. As the field increases and the cyclotron diameter d_c is less than the wire diameter ($d_c < d$), boundary scattering becomes ineffective and the resistance decreases. According to the theory, the resistance of the NW decreases, approaching a limiting value of $R = L/[\sigma(T)A]$, where $A=(\pi/4)d^2$ is the cross-sectional area of the NW and $\sigma(T)$ is the conductivity of bulk Bi. The magnetoresistance is therefore negative. However, if the NW material has a nonzero, (bulk) positive LMR, the resulting LMR shows a mixed behavior with a maximum occurring, very roughly, for a magnetic field B_c. In practice, any misalignment results in a shift of the LMR maximum to higher fields.

Figure 5 shows that the LMR is decorated with SdH

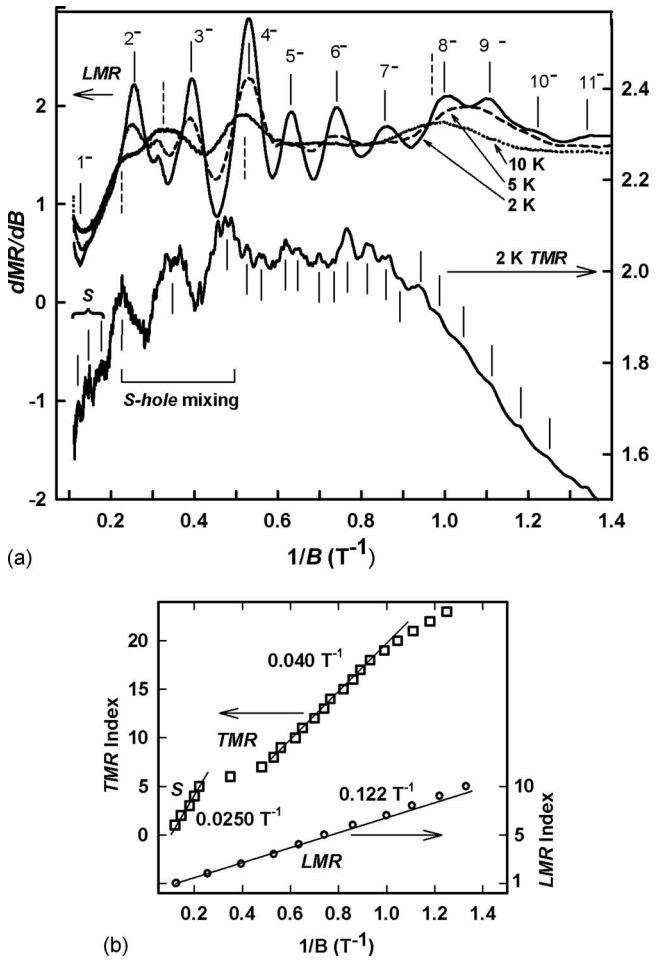

FIG. 6. (Top) Derivatives of the LMR and TMR of the 200 nm (nominal) Bi NWA at various temperatures (as indicated) as a function of $1/B$. The vertical lines indicate the Landau levels. The dashed vertical lines indicate the peaks of a sequence with a period of 0.31 T^{-1}. Peaks are holes unless explicitly indicated to be electrons. *S* stands for surface. For the LMR hole LSs, n^- represents a doublet of n^- and $(n-2)^+$ except for the 1^- that is a singlet; for example, the 2^- is accompanied by the 0^+. (Bottom) $1/B$ index of the peaks shown with vertical lines.

oscillations. The presence of SdH oscillation resonances is more apparent in a plot of the derivative of the LMR versus $1/B$. Figure 6 shows $d\mathrm{LMR}/dB$ and $d\mathrm{TMR}/dB$ for $B > 0.7$ T at various temperatures. SdH oscillations are caused by the quantization of closed orbits also called Landau states. As the magnetic field is increased, the energy of the Landau states (LS), i.e., Landau levels, increases, and when one of their values becomes equal to the Fermi energy, this level starts being depopulated. The relaxation time for electron scattering is temporarily increased at this field value, giving rise to a dip in the magnetoresistance. The LMR data show a number of minima and short-period oscillations. The SdH minima corresponding to holes in a bulk Bi single crystal were studied by Smith *et al.*[36] and by Brown.[37] The accepted value for the SdH period for hole carrier doublets in bulk Bi $P_{h,\|}$ (bulk) is 0.157 T^{-1}. Recently, Bompadre *et al.*[38] studied the spin splitting of the peaks in this sequence. The period of the peaks that we observe is $P_{h,\|}(\mathrm{NWs})=0.12\pm0.01$ T^{-1}. Accordingly, the peaks that we observe can be indexed in terms of quantum number and spin, as shown by Smith *et al.*[36] For example, the peak at 0.42 T^{-1} is the 3^-, 1^+ pair.

According to this correspondence, the strong feature at 0.125 T^{-1} is associated with the 1^-, which is a singlet at the hole quantum limit (there are no hole LS eigenstates at higher magnetic fields). This feature can be observed in the LMR shown in Fig. 5 directly, where it is indicated with a vertical arrow.

At high temperatures and low magnetic fields the hole SdH oscillations continue as a sequence of peaks with a period of approximately 0.31 ± 0.02 T^{-1}. This sequence is more clearly observed for $T=10$ K. A plausible origin for a SdH period of 0.3 T^{-1} may be that our NWs have a distribution of angles relative to the Anapore surface normal and therefore with respect to the magnetic field. If the degree of misalignment is as high as 20°, electron SdH oscillations, which have a reported period[39] of 0.30 T^{-1}, should be observable. This is consistent with the degree of misalignment of the NWs as shown in Fig. 2. The misalignment is probably compounded by the difficulty in exactly aligning our small samples in the applied magnetic field. Assuming that there is a distribution of orientations, we can correct our estimate of the confinement-induced decrease in the SdH hole period. The angular variation of the hole periods in the binary plane has been measured,[39] and for a distribution of angles between 20° and −20° around the trigonal direction, the average hole period is 0.152 T^{-1}. Therefore, since the observed holes' SdH period is 0.122 T^{-1}, the value for the shift of period of the LMR, $\Delta P_{h,\|}$, is −0.03 with a deviation of ± 0.01 T^{-1} from the expected value for bulk Bi.

Figure 6, top, also shows the derivative of the TMR for $B>0.7$ T at 1.8 K with a number of short-period oscillations that are indicated with vertical lines. There are two main sequences for $B^{-1}<0.22$ T^{-1} and for $B^{-1}>0.53$ T^{-1}, which are characterized by periods $P_{h,\perp}(\mathrm{NW},1)=0.025$ T^{-1} and $P_{h,\perp}(\mathrm{NW},2)=0.048$ T^{-1}, respectively; the former sequence is very noisy. The 0.13 T^{-1} long period observed in the range $0.22-0.53$ T^{-1} is the beating of the two short periods. The TMR SdH for hole carriers in a bulk Bi single crystal have been studied.[36,39,40] The accepted value for the SdH period for hole carriers in bulk Bi, $P_{h,\perp}$, is 0.046 T^{-1}. The hole SdH period for B near the perpendicular to the trigonal axis (C3) is not a sensitive function of angle (because spin splitting increases for orientations away from the binary-bisectrix plane) as in the LMR case. The sequence with a period of 0.025 T^{-1} could be interpreted in terms of an electron contribution in NWs in the array that are aligned so that the binary axis is parallel to the magnetic field. This signal was observed by Smith *et al.*[36] Alternatively, the 0.025 T^{-1} can be interpreted also in terms of surface states.[11,13]

The hole SdH periods differ from the accepted value for bulk Bi, as follows. From Fig. 6 the hole Fermi surface can be interpreted in terms of the ellipsoidal model. The hole number density for an ellipsoidal Fermi surface is given by the equation[10]

$$p = (8/3\pi^{1/2})\Phi_0^{-3/2}(P_{h,\|}P_{h,\perp}{}^2)^{-1/2}, \quad (1)$$

where $\Phi_0=hc/e$. As previously noted, for bulk single-crystal Bi, $P_{h,\|}=0.157$ T^{-1} $(B\|\mathrm{C3})$ and $P_{h,\perp}=0.045$ T^{-1} $(B\perp\mathrm{C3})$. Therefore, one finds $p=3.0\times10^{17}/\mathrm{cm}^3$. For our NWs, where $P_{h,\|}=0.122$ T^{-1} $(B\|\mathrm{C3})$ and $P_{h,\perp}=0.048$ T^{-1} $(B\perp\mathrm{C3})$, we find that $p=3.15\pm0.3\times10^{17}/\mathrm{cm}^3$. Therefore, within the margin of error, p is not modified by quantum confinement. In our previous study[10] of Landau levels in NWAs, p was found to decrease slightly, by 13%, consistently with quantum confinement. Also, in Ref. 13, it was observed that the hole Fermi surface ellipsoid was less anisotropic in NWs. Here we observe the same trend.

In this section we have shown that the samples have well developed SdH oscillations, which are only observed in bulk Bi samples of high quality. Qualitatively, such a case indicates that the samples have very high intrinsic mobility, since Landau states can be understood as circular orbits, whenever carriers avoid collision with the walls.[40]

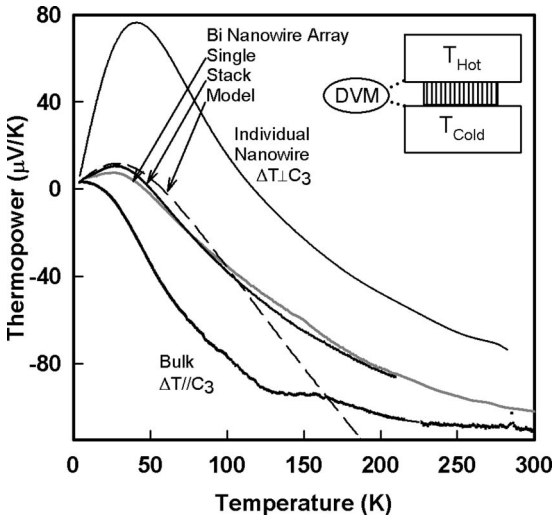

FIG. 7. Thermopowers of the Bi NWAs and single-crystal Bi samples oriented with C3 parallel to the temperature gradient as a function of temperature. The data corresponding to single NWAs and stacks formed with three NWAs in series are indicated. The data for individual Bi NWs are adapted from Ref. 15. The thermopower of single-crystal Bi NWs with C3 $\perp \Delta T$ was adapted from Ref. 20. The inset shows the setup employed for our thermopower measurements, which is of the anvil type. ΔV indicates the voltmeter that is used to measure the thermoelectric voltage generated by the temperature difference between T_{hot} and T_{cold}.

IV. THERMOPOWER RESULTS AND MODEL

A discussion of the relevance and shortcomings of thermopower as an experimental probe is found in Ref. 41. The inset in Fig. 7 illustrates the experimental setup. This device was mounted in a closed cycle refrigerator with a temperature range from 4 K to room temperature. NWA samples, which were a fraction of a millimeter thick and with a surface area ~1 mm^2, were contacted through the anvil pieces using In foil or silver paint as an interface material. The heater allowed us to create a temperature difference between the two electrodes and therefore between the two ends of the wires. Figure 7 presents our data for the thermopower α as well as data from other sources. $\alpha=\Delta V/\Delta T$, where ΔV is the electric potential generated across the NW in response to temperature difference $\Delta T=T_{\mathrm{hot}}-T_{\mathrm{cold}}$ between the NW ends. During experimental runs we simultaneously measure α and R as a function of temperature in the range 4–300 K for $B=0$ and for $B=0.4$ T. The measurements in a magnetic field allow us to verify the resistance of the samples. As a

check, the thermopower of a single crystal of high purity Bi ($\Delta T \| C3$) was measured with the same method. The results are also shown in Fig. 7; our measurements agree with previous determinations of the thermopower of bulk Bi in this orientation.[20] There are two important features common to all the 200 nm NWA samples that we have measured. First, α is positive at low temperatures. It changes sign from negative to positive between 100 and 200 K, and it exhibits a peak at around 50 K. Second, we found that the thermopower at room temperature was close to that of bulk Bi for the crystalline orientation of the NWs. Our measurements are not unlike the measurements of 200 nm Bi NWAs by Heremans and Thrush,[6] where the thermopower of 200 nm pure Bi NWAs was found to be negative for $T>40$ K and positive for $T<40$ K, and a small positive peak (3 ± 1 μV/K) was observed at intermediate temperatures at around 20 K. However, in our measurements, the positive maximum is more pronounced. In this regard the thermopower of 200 nm samples is similar to that for individual Bi NWs.[15]

The resistance and thermopower effects that we observe are interpreted together, on an equal footing, in terms of size effects within the framework derived from the Boltzmann equation. In this framework, the resistance and thermopower are functions of the carrier's densities and mobilities. To this formal framework, we incorporate our knowledge of the carrier's densities and a simple model of the NW carrier's mobilities, which takes into account the restriction to the mfp by the boundaries.

The phenomenological theory of low-field galvanometric effects in Bi in terms of carrier density and mobilities is derived from the Boltzmann equation[42] with Ohm's law holding for the resistivity tensor. This tensor must be invariant under the point symmetry operations of the crystal. This condition restricts the number of nonzero elements in the resistivity tensor to 6, and the number of independent and large components of the mobility tensor for electrons and holes to 3 and 2, respectively. μ_1, μ_2, and μ_3 are electron mobilities, and ν_1 and ν_3 are the hole mobilities. The resistance, as well as the thermopower, of a macroscopic long cylinder of Bi obeys the Thomson–Voigt relation as presented by Gallo *et al.*[20] For instance, $R=R_\perp \sin^2\beta + R_\| \cos^2\beta$. Here β is the angle between the cylinder axis and the trigonal direction, and $\perp$ and $\|$ denote cylinder orientations perpendicular and parallel to the trigonal axis. Because the NWs are oriented preferentially along the C3 axis, our case is simple and corresponds approximately to the parallel one. From Ref. 42, the partial conductivities of electrons $\sigma_e(=1/\rho_e)$ and holes $\sigma_h(=1/\rho_h)$ are

$$\sigma_e = en\mu_3 \tag{2}$$

and

$$\sigma_h = ep\nu_3, \tag{3}$$

where n and p are the electron and hole carrier densities, respectively. Here $\rho=1/(\sigma_e+\sigma_h)$. In the diffusive case, we find that the thermopower, a scalar, is an average of the partial thermopowers of electrons and holes, weighted according to the partial electric conductivities

$$\alpha = (\alpha_e\sigma_e + \alpha_h\sigma_h)/(\sigma_e + \sigma_h), \tag{4}$$

where α_e and α_h are the partial thermopowers of the electrons and holes, and $\alpha_e<0$ and $\alpha_h>0$. The sign of the partial thermopower is related unambiguously to the sign of the charge of the carriers, and consequently the thermopower is instrumental in establishing the type of conductivity (type n or type p).

The values of the partial thermopowers can be calculated from the electron and hole band parameters. We have shown that confinement introduced only small modifications in these parameters from the bulk values, and we will use the band parameters from bulk Bi. Askerov obtained the partial electron and hole thermopowers for a degenerate semiconductor in the Boltzmann approximation for isotropic parabolic bands.[43] These are given by

$$\alpha_e = -\left(\frac{k_B^2\pi^2T}{3e}\right)\left[(r+1)\frac{(E_g^L+2E_F^e)}{E_F^e(E_g^L+E_F^e)} - \frac{4}{(E_g^L+2E_F^e)}\right],$$

$$\alpha_h = \left(\frac{k_B^2\pi^2T}{3e}\right)\left[\frac{(r+1)}{E_F^h}\right], \tag{5}$$

where r is the exponent of the temperature dependence of the phonon part of the resistance. $E_g^L=15.3$ meV is the L-electron-hole gap. Further, $E_F^e=27$ meV and $E_F^h=11$ meV are the electron and hole Fermi energies. The partial thermopower expressions apply in the nondegenerate case, where k_BT is much less than the Fermi energies.

Heremans and Hansen[22] derived a different expression for α_e for the case of the NWs, where scattering on the wall dominates.

$$\alpha_e = -\left(\frac{k_B^2\pi^2T}{3e}\right)\frac{(E_g^L+2E_F^e)}{E_F^e(E_g^L+E_F^e)}. \tag{6}$$

Taking the values appropriate for bulk Bi, $r=\frac{1}{2}$, and using Eq. (5), we find $\alpha_e=-0.81\pm0.1$ T μV/K^2 and $\alpha_h=3.39\pm0.3$ T μV/K^2. According to Eq. (6), $\alpha_e=-1.48\pm0.1$ T μV/K^2. The errors are related to the uncertainty regarding the Fermi energies.

The rest of this section deals with the interpretation of resistance and thermopower size effects in terms of a simple model of mobilities. In this model, the carrier mobility has a mixed behavior; at high temperatures, the mobility increases for decreasing temperatures similar to the bulk, and at intermediate temperatures the mobility saturates, becoming a constant at low temperatures. The total carrier mobility in NWs by various scattering processes can be described as follows:

$$\mu_3^{NW} = (\mu_3^{-1} + \mu_b^{-1})^{-1}, \tag{7}$$

$$\nu_3^{NW} = (\nu_3^{-1} + \nu_b^{-1})^{-1}, \tag{8}$$

where μ_3^{NW} and ν_3^{NW} are the NWs' electron and hole mobilities, respectively. The electron and hole mobilities of bulk Bi have been determined.[23,42] At 77 K, $\mu_3=39$ m^2 V^{-1} s^{-1} and $\nu_3=0.56$ m^2 V^{-1} s^{-1}. In bulk Bi, mobilities increase for decreasing temperature as $T^{-1.5}$ achieving, at 4 K, values of $\mu_3=6800$ m^2 V^{-1} s^{-1} and $\nu_3=350$ m^2 V^{-1} s^{-1}. μ_b and ν_b ac-

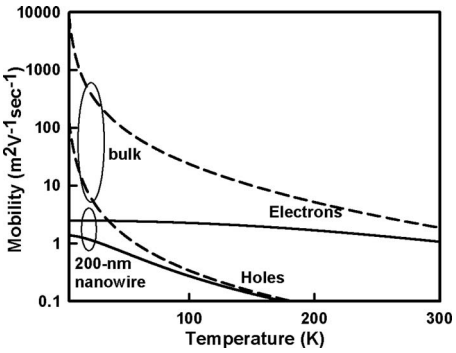

FIG. 8. Temperature-dependent electron μ_3 and hole ν_3 mobilities in the model based on Eqs. (2)–(8). μ_b=3.5 $m^2\ V^{-1}\ s^{-1}$ and ν_b=1.5 $m^2\ V^{-1}\ s^{-1}$. As indicated, solid lines correspond to 200 nm NW and dashed line to bulk Bi.

count for the boundary scattering of electrons and holes, respectively. In this way, surface effects can be discussed without specific reference to, but including, specular boundary scattering that is parametrized by the specularity coefficient. This simple model of mobilities, implicit in Eqs. (2)–(8), was found to be useful in the interpretation of individual Bi NW data by NHGK.[15]

The resistance and thermopower data for 200 nm wires in Figs. 4 and 7 are fitted by μ_b=3.5 $m^2\ V^{-1}\ s^{-1}$ and ν_b =1.5 $m^2\ V^{-1}\ s^{-1}$. Figure 8 shows the temperature-dependent mobilities according to this model. At high temperatures, the bulk contribution to μ and ν becomes dominant, $\mu > \nu$, and the thermopower is negative and roughly equal to that of bulk Bi (as observed). At room temperature, the resistance of the NWs is roughly equal to that calculated from the bulk Bi resistivity; this is also consistent with our data. Since the results of our model for Bi NWs indicate that the total mobility of holes approaches that of electrons at low temperatures ($T<80$ K), the peak of the thermopower, at around 40 K, is associated with the interplay between bulk and surface contributions to the mobility. We note that the model reproduces the anomalous inflection point near 50 K in the temperature dependence of the resistance.

V. DISCUSSION IN TERMS OF BOUNDARY SCATTERING THEORIES

Although our thermopower measurement results are roughly consistent with those by Heremans and Thrush,[6] our interpretation with a diffusion thermopower model is a sharp departure from their interpretation in terms of phonon drag. Considering experimental errors and the simplicity of our model, our interpretation is strengthened by the simultaneous fit to the thermopower data and the essential features of the resistance. It indicates that mobility limitations posed by hole-boundary scattering are much less severe than those due to electron-hole scattering. For temperatures below the thermopower maximum, since the carrier density is temperature independent, $\alpha=(\alpha_e\mu_b+\alpha_h\nu_b)/(\mu_b+\nu_b)$ and the thermopower is linear with temperature, as observed.

Finite size effects appear when $d<$mfp. Heremans *et al.*[44] presented the expression for the electron and hole mfp. This expression can be written as

$$\mathrm{mfp}_e = (h/e) \times \frac{\mu_3}{\lambda_F^e}, \tag{9}$$

where $\lambda_F^e=2\pi/k_F^e$. k_F^e, the Fermi momentum of electrons for this NW, is $[2m_l\gamma(E_F^e)]^{1/2}/\hbar$. $\gamma(E_F^e)=E_F^e(1+E_F^e/E_g^L)$ corrects the electron Fermi energy to take into account nonparabolicity effects. The corresponding expression for the hole mfp is

$$\mathrm{mfp}_h = (h/e) \times \frac{\nu_3}{\lambda_F^h}, \tag{10}$$

where $\lambda_F^h=\hbar(2M_lE_F^h)^{-1/2}$ and M_l is the longitudinal hole mass.

The quasiparticle, longitudinal and cyclotron, masses of the NWs are the same ones that would be obtained for a bulk single crystal with the same orientation. We know this because the Fermi surface parameters were measured for our NWs and found to be the same as for the bulk (see Sec. III). The subject of Bi carrier masses has been discussed extensively.[36,42] For the samples in the present work, the hole longitudinal mass M_l is 0.69 and the electron longitudinal mass m_l is 0.02. The cyclotron electron m_c and hole M_c masses are 0.065 and 0.067, respectively, that is, approximately the same. The masses are normalized with respect to the value of the free electron mass. We find λ_F^e=31 nm and λ_F^h=14 nm. As indicated in Sec. IV, in bulk Bi, at 4 K, values of μ_3=6800 $m^2\ V^{-1}\ s^{-1}$ and ν_3=350 $m^2\ V^{-1}\ s^{-1}$ were achieved. Using expressions (9) and (10), one finds that the low-temperature mfps of electrons and holes in bulk Bi are 1.3 mm and 100 μm, respectively.[45] For the 240 nm individual Bi NWs in Ref. 15, with a hole mobility of 50 $m^2\ V^{-1}\ s^{-1}$, we find mfp_h=3 μm. For the 200 nm Bi NWs here, we find mfp_h=0.4 μm and mfp_e=0.5 μm. Clearly, for both holes and electrons mfp$>d$, which appears at first glance to be an unphysical result. This may be explained by specular boundary scattering, that is, $\varepsilon>0$, within the Fuchs–Sondheimer approach and for carrier mfp much smaller than that of the carrier in the bulk. In this case, an increase in ε has the effect of increasing the conductivity and mobilities, and consequently [see Eqs. (9) and (10)], the mfp. Still, considering the diverse models of size effects that have been proposed, this interpretation in terms of ε is preliminary, at best, because it does not consider the mechanism for scattering.

The weak dependence of the boundary mobility on quasiparticle mass that we observe can be interpreted in terms of Fishman and Calecki[30,31] theory of boundary roughness scattering and Bergmann's diffraction theory.[32] Fishman and Calecki[30,31] assumed that $\lambda_F \gg \zeta$, where ζ is the correlation length describing the surface roughness. Bismuth NWs fall in the metallic case since the number of subbands open for conduction, N, is much greater than one. $N \approx (3n/\pi)^{1/3}d$ =15 for 200 nm NWs. In the metallic case, for a single pocket with parabolic dispersion, Fishman and Calecki[30,31] found that the conductivity for a given n, and therefore the mobility, is independent of both the cyclotron mass (the cyclotron mass is hidden in N and the Fermi wavevector of a channel k_F) and the longitudinal mass of the carriers. Bergmann[32] found that the limiting mfp is W^2/λ_F where W is the film width and λ_F is the Fermi wavelength. We believe

that the λ_F should be calculated from the longitudinal mass, and not the cyclotron mass, because it is this mass that is involved in wavelike propagation forward into the film. Therefore, it is simple to show using the relation between mobility and mfp [Eqs. (9) and (10)] that in our framework, Bergmann's[32] result is that the mobility is independent of longitudinal mass, same as by Fishman and Calecki.[30,31]

Our detailed analysis of our experimental results for the dependence of the mobility on the longitudinal masses is as follows. In our case, the case of trigonal Bi NWs, the three electron pockets in the Fermi surface are equivalent and the ratio of the hole longitudinal mass to electron longitudinal mass is 35. The ratio μ_b/ν_b of the electron and hole mobilities in the experiment, which are $\mu_b=3.5\ \mathrm{m^2\ V^{-1}\ s^{-1}}$ and $\nu_b=1.5\ \mathrm{m^2\ V^{-1}\ s^{-1}}$, is only 2.3 (in comparison, in bulk Bi $\mu_3/\nu_3 \sim 30$). Therefore, we find that the mobilities depend very weakly on longitudinal mass in qualitative agreement with both the theory of Fishman and Calecki[30,31] and that of Bergmann.[32] However, neither of these theories of boundary scattering can account for the observations quantitatively since in these theories the mobilities are completely independent of mass, and therefore of the Fermi wavelength, which is contrary to the experiments because we observe a small deviation, $(\mu_b-\nu_b)$. A possible explanation is that the inequality $\lambda_F \gg \zeta$ is not satisfied; in other words, the spectrum of roughness is not flat. Regarding an estimate of the extent of the roughness in our NWs, we have examined cross sections of NWAs in SEM images of the type shown in Fig. 2. We do observe various irregularities that qualify as roughness within the experimental resolution that is 30 nm. Moreover, Fishman and Calecki[30,31] pointed out that, in some experiments where a significant surface roughness scattering is observed in the conductivity, topographic examination of the surface reveals it to be rough only at the atomic scale.

A computer model study of the charge carrier mobility in Si NWs with rough surfaces has been presented; it was found that the mobilities are weakly dependent on the carrier type.[46] Our results may suggest strategies, based on the Fermi surface properties of the conductors, for minimizing finite-size effects in the electrical resistance of submicron metal interconnects of semiconductor devices. Our results are also relevant in the field of solid-state heat-to-electric energy conversion since finite-size effects promote, indirectly, thermopower size effects.

Our model, in particular, Eqs. (7) and (8), assumes the validity of Matthiessen's rule and this validity has been questioned for surface roughness scattering.[47] However, Eqs. (7) and (8) are simply an artifice to model mathematically the switching between the low-temperature and the high-temperature regimes.

VI. SUMMARY AND CONCLUSIONS

We present an experimental study of size effects on electronic transport in Bi NWs. Resistance, magnetoresistance, and thermopower of bismuth NWs were measured. Numerical simulations of the resistance and diffusive thermopower, taking into account both bulk and surface boundary scattering processes, allow us to extract the electron and hole charge carrier mobilities from our data. The temperature-independent term that limits the carrier mobility is obtained and the issue of the mass dependence of boundary scattering is addressed experimentally. The weak dependence of the boundary mobility on quasiparticle mass that we observe is interpreted in terms of Fishman and Calecki's[30,31] theory of boundary roughness scattering and Bergmann's[32] diffraction theory.

ACKNOWLEDGMENTS

We wish to thank Professor Gerd Bergman for enlightening discussions on finite-size effects. T.E.H. and M.J.G.'s work was supported by the Division of Materials Research of the U.S. National Science Foundation under Grant Nos. NSF-0611595 and NSF-0506842. T.E.H.'s work was also sponsored by the Division of Materials of the U.S. Army Research Office under Grant No. DAAD4006-MS-SAH. This work was supported by Civilian Research and Development Foundation for the Independent States of the Former Soviet Union (CRDF), Grant No. MP2–3019.

[1] M. S. Dresselhaus, Y. M. Lin, O. Rabin, A. Jorio, A. G. Souza Filho, M. A. Pimenta, R. Saito, G. Samsonidze, and G. Dresselhaus, Mater. Sci. Eng., C **23**, 129 (2003).
[2] D. G. Cahill, W. K. Ford, K. E. Goodson, G. D. Mahan, A. Majumdar, H. J. Maris, R. Merlin, and S. R. Phillpot, J. Appl. Phys. **93**, 793 (2003).
[3] L. D. Hicks and M. S. Dresselhaus, Phys. Rev. B **47**, 12727 (1993).
[4] H. J. Goldsmid, *Electronic Refrigeration* (Pion Limited, London, 1986).
[5] Z. Zhang, X. Sun, M. S. Dresselhaus, and J. Y. Ying, Appl. Phys. Lett. **73**, 1589 (1998).
[6] J. Heremans and C. M. Thrush, Phys. Rev. B **59**, 12579 (1999). Expressions (8) and (9) for the Seebeck coefficients of electrons and holes have an error; the exponent of the temperature, which is shown to be T^2, should be T.
[7] T. E. Huber, O. Anakoya, and M. Ervin, J. Appl. Phys. **92**, 1337 (2002).
[8] J. G. Rodrigo, A. Garcia-Martin, J. J. Saenz, and S. Vieira, Phys. Rev. Lett. **88**, 246801 (2002).
[9] Y.-M. Lin, S. B. Cronin, J. Y. Ying, and M. S. Dresselhaus, Appl. Phys. Lett. **76**, 3944 (2000).
[10] T. E. Huber, K. Celestine, and M. J. Graf, Phys. Rev. B **67**, 245317 (2003).
[11] T. E. Huber, A. Nikolaeva, D. Gitsu, L. Konopko, C. A. Foss, and M. J. Graf, Appl. Phys. Lett. **84**, 1326 (2004).
[12] A. Boukai, K. Xu, and J. R. Heath, Adv. Mater. (Weinheim, Ger.) **18**, 864 (2006).
[13] T. E. Huber, A. Nikolaeva, D. Gitsu, L. Konopko, and M. J. Graf, Physica E (Amsterdam) **37**, 194 (2007).
[14] T. W. Cornelius, M. E. Toimil Molares, R. Neumann, and S. Karim, J. Appl. Phys. **100**, 114307 (2006).
[15] A. Nikolaeva, T. E. Huber, D. Gitsu, and L. Konopko, Phys. Rev. B **77**, 035422 (2008).
[16] I. Ya. Korenblit, M. E. Kuznetov, and S. S. Shalyt, Zh. Eksp. Teor. Fiz. **56**, 8 (1969) [Sov. Phys. JETP **29**, 4 (1969)].
[17] V. A. Kozlov and E. L. Nagaev, JETP Lett. **13**, 455 (1971) [Pis'ma Zh. Eksp. Teor. Fiz. **13**, 639 (1971)].
[18] V. N. Kopilov and L. Meshov-Deglin, Zh. Eksp. Teor. Fiz. **38**, 357 (1973) [Sov. Phys. JETP **65**, 720 (1973)].
[19] D. Gitsu, T. Huber, L. Konopko, and A. Nikolaeva, Phys. Status Solidi B **242**, 2497 (2005).
[20] C. F. Gallo, B. S. Chandrasekhar, and P. H. Sutter, J. Appl. Phys. **34**, 144 (1963).
[21] O. P. Hansen, E. Cherurier, J.-P. Michenaud, and J.-P. Issi, J. Phys. C **11**, 1825 (1978).
[22] J. Heremans and O. P. Hansen, J. Phys. C **12**, 3483 (1979).
[23] J.-P. Issi, Aust. J. Phys. **32**, 585 (1979).
[24] W. Kraak, R. Herrmann, and H. Haupt, Phys. Status Solidi B **109**, 785 (1982).
[25] J. F. Nye, *Physical Properties of Crystals* (Oxford University Press, London, 1960), pp. 24–26, 195–200, and 204–207.

[26]K. Fuchs, Proc. Cambridge Philos. Soc. **34**, 100 (1938).
[27]E. H. Sondheimer, Adv. Phys. **1**, 1 (1952).
[28]R. B. Dingle, Proc. R. Soc. London, Ser. A **201**, 545 (1950).
[29]W. Steinhögl, G. Schindler, G. Steinlesberger, and M. Engelhardt, Phys. Rev. B **66**, 075414 (2002).
[30]G. Fishman and D. Calecki, Phys. Rev. Lett. **62**, 1302 (1989).
[31]G. Fishman and D. Calecki, Phys. Rev. B **43**, 11581 (1991).
[32]G. Bergmann, Phys. Rev. Lett. **94**, 106801 (2005).
[33]A. Suzuki, Y. Hasegawa, Y. Ishikawa, and T. Komine, Rev. Sci. Instrum. **76**, 023907 (2005).
[34]R. G. Chambers, Proc. R. Soc. London, Ser. A **202**, 378 (1950).
[35]V. Sundaram and A. Mizel, J. Phys.: Condens. Matter **16**, 4697 (2004).
[36]G. E. Smith, G. A. Baraf, and J. M. Rowell, Phys. Rev. **135**, A1118 (1964).
[37]R. D. Brown III, Phys. Rev. B **2**, 928 (1970).
[38]S. G. Bompadre, C. Biaginni, D. Maslov, and A. F. Hebard, Phys. Rev. B **64**, 073103 (2001).
[39]L. S. Lerner, Phys. Rev. **127**, 1480 (1962).
[40]R. J. Balcombe and A. M. Forrest, Phys. Rev. **151**, 550 (1966).
[41]N. W. Ashcroft and N. D. Mermin, *Solid State Physics* (Harcourt Brace College, 1976), Chap. 14.
[42]R. Hartman, Phys. Rev. **181**, 1070 (1969).
[43]B. M. Askerov, *Electron Transport Phenomena in Semiconductors* (World Scientific, Singapore, 1994), p. 183.
[44]J. Heremans, C. M. Thrush, Y.-M. Lin, S. Cronin, Z. Zhang, M. S. Dresselhaus, and J. F. Mansfield, Phys. Rev. B **61**, 2921 (2000).
[45]In Hartman's work (Ref. 42) at low temperatures, the electron mfp is comparable with the sample size. This was noted by the author. A saturation of μ_1 was observed. The phenomenon of saturation of the electronic mobilities in millimeter-size samples has been discussed more recently in W. Kraak, R. Kuhl, F. Thom, H. Haefner, and P. Schmidt, Phys. Status Solidi B **105**, 597 (1981).
[46]A. Lherbier, M. P. Persson, Y.-M. Niquet, F. Triozon, and S. Roche, Phys. Rev. B **77**, 085301 (2008).
[47]R. C. Munoz, A. Arenias, G. Kremer, and L. Moraga, J. Phys.: Condens. Matter **15**, L177 (2003).